THE JOURNAL OF PHYSICAL CHEMISTRY Letters

Letter

Cite This: J. Phys. Chem. Lett. 2017, 8, 6154−6159

pubs.acs.org/JPCL

How Strong Is the Hydrogen Bond in Hybrid Perovskites?

Katrine L. Svane,[†] Alexander C. Forse,[‡,▽] Clare P. Grey,[‡] Gregor Kieslich,[§] Anthony K. Cheetham,[∥] Aron Walsh,[⊥,#] and Keith T. Butler*[,†]

[†]Department of Chemistry, University of Bath, Bath BA2 7AY, United Kingdom

[‡]Department of Chemistry, Cambridge University, Cambridge CB2 1EW, United Kingdom

[§]Department of Chemistry, Technical University of Munich, Lichtenbergstraße 4, 85748 Garching, Germany

[∥]Department of Materials Science and Metallurgy, University of Cambridge, Cambridge CB3 0FS, United Kingdom

[⊥]Department of Materials, Imperial College London, Exhibition Road, London SW7 2AZ, United Kingdom

[#]Department of Materials Science and Engineering, Yonsei University, Seoul 03722, Korea

Supporting Information

ABSTRACT: Hybrid organic−inorganic perovskites represent a special class of metal−organic framework where a molecular cation is encased in an anionic cage. The molecule−cage interaction influences phase stability, phase transformations, and the molecular dynamics. We examine the hydrogen bonding in four $AmBX_3$ formate perovskites: $[Am]Zn(HCOO)_3$, with Am^+ = hydrazinium ($NH_2NH_3^+$), guanidinium ($C(NH_2)_3^+$), dimethylammonium $(CH_3)_2NH_2^+$, and azetidinium $(CH_2)_3NH_2^+$. We develop a scheme to quantify the strength of hydrogen bonding in these systems from first-principles, which separates the electrostatic interactions between the amine (Am^+) and the BX_3^- cage. The hydrogen-bonding strengths of formate perovskites range from 0.36 to 1.40 eV/cation (8−32 kcalmol^{-1}). Complementary solid-state nuclear magnetic resonance spectroscopy confirms that strong hydrogen bonding hinders cation mobility. Application of the procedure to hybrid lead halide perovskites (X = Cl, Br, I, $Am^+ = CH_3NH_3^+$, $CH(NH_2)_2^+$) shows that these compounds have significantly weaker hydrogen-bonding energies of 0.09 to 0.27 eV/cation (2−6 kcalmol^{-1}), correlating with lower order−disorder transition temperatures.

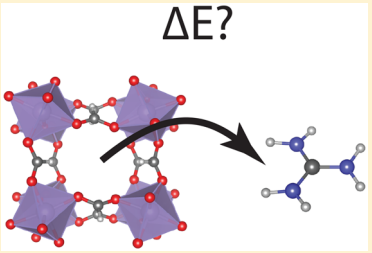

Organic−inorganic perovskites have risen to prominence within the area of material science over the past decade.[1] Hybrid perovskites with the general formula ABX_3 exhibit many fascinating properties, ranging from (multi)ferroics[2,3] to photovoltaics and light-emitting applications.[4] This range of physical properties is accessible by appropriate choice of chemical components due to the large compositional adaptability of the perovskite-motif, and further fine-tuning can be achieved by the formation of solid solutions.[5,6] While this is also true for inorganic perovskites, the soft intermolecular interactions in hybrid organic−inorganic perovskites give rise to unique phenomena. Recent studies within the field have focused on lattice dynamics,[7] revealing striking insight into the underlying structure−property relationships, for example, dynamic and local symmetry-breaking phenomena,[8,9] unusual thermal expansion behavior[7,10] and the role of lattice entropy.[11] In particular, hydrogen bonding has been identified as a source of low-frequency lattice modes, giving rise to important contributions to the relative stability of different phases.[12]

When studying the impact of hydrogen bonding and weak chemical interactions on the macroscopic properties of hybrid compounds, formate perovskites with the general formula $[Am]M[(CHOO)_3]$ represent an ideal test set.[13] In these materials, (divalent) metal atoms M are bridged by formate ions to form a ReO_3-type cavity within which the amine cations ([Am]) reside. Importantly, the amine cation can chemically interact with the negatively charged cavity through both nondirectional electrostatic interactions and directional hydrogen bonds, the latter inherently absent in purely inorganic materials. These relatively weak interactions often lead to orientational ordering of the cations at low temperatures, which for some compounds is associated with (anti)ferroelectric properties.[14−17] However, thermal motion eventually allows reorientation of the cation at some finite temperature, T_c, that depends on its identity, leading to an order−disorder phase transition.[11,12] The hydrogen bonding also influences other material properties. For instance, when comparing $[C(NH_2)_3]Mn(HCOO)_3$ and $[(CH_3)_2NH_2]Mn(HCOO)_3$, the number of hydrogen-bonding interactions can be qualitatively linked to their mechanical properties.[18]

Hydrogen bonding is of eminent importance in biological systems, with protein folding and the pairing of DNA bases as some of the most prominent examples.[19] It is therefore not surprising that, when present, it also affects the properties of solids. Hydrogen bonds are directional interactions involving a polar donor group $X^{\delta-}-H^{\delta+}$ and an electronegative atom $A^{\delta-}$. Prototypical H bonds such as the O−H−O bond in water and the N−H−O bond in proteins are largely electrostatic in

Received: November 23, 2017
Accepted: December 8, 2017
Published: December 8, 2017

DOI: 10.1021/acs.jpclett.7b03106
J. Phys. Chem. Lett. 2017, 8, 6154−6159

nature; however, the hydrogen bond merges continuously with van der Waals interactions and ionic and covalent bonds.[20,21] Neither computational nor experimental methods can easily deconvolute the individual contributions to the energy, and reported hydrogen-bonding energies are therefore typically based on dimerization energies, which include all of these interactions. In the case of hydrogen bonding between charged species the energy will often be dominated by the ionic (monopole) part of the electrostatic interaction, which is independent of the relative orientation of the ions. In the following, we are interested in the orientation-dependent component of the bonding and use the term hydrogen bonding to refer to electrostatic interactions from dipolar and higher-order terms.

In this study, we develop a first-principles scheme to quantify the hydrogen-bonding strength in hybrid perovskites. We apply the scheme to four formate perovskites $[C(NH_2)_3]Zn(HCOO)_3$ (**Gua**$^+$), $[NH_2NH_3]Zn(HCOO)_3$ (**Hy**$^+$), $[(CH_2)_3NH_2]Zn(HCOO)_3$ (**Aze**$^+$), and $[(CH_2)_2NH_2]Zn(HCOO)_3$ (**Dma**$^+$) (see Figure 1), where the cations differ in the number of potential hydrogen bonds and the degree of cation motion. The results are validated by experimental results obtained by solid-state ^{1}H nuclear magnetic resonance (^{1}H NMR), which gives information about cation dynamics. We then apply the scheme to the family of hybrid lead halide perovskites based on the halides Cl, Br, I, and the CH_3NH_3 (**Ma**$^+$) and $CH(NH_2)_2$ (**Fa**$^+$) cations, showing that the hydrogen bonding in these materials is significantly weaker than in the formate perovskites, in accordance with their lower order−disorder transition temperature. The results demonstrate that our approach provides a quantitative assessment of the forces that determine the physical properties in organic−inorganic systems, constituting a valuable tool in the development of structure−property relationships in this important class of materials.

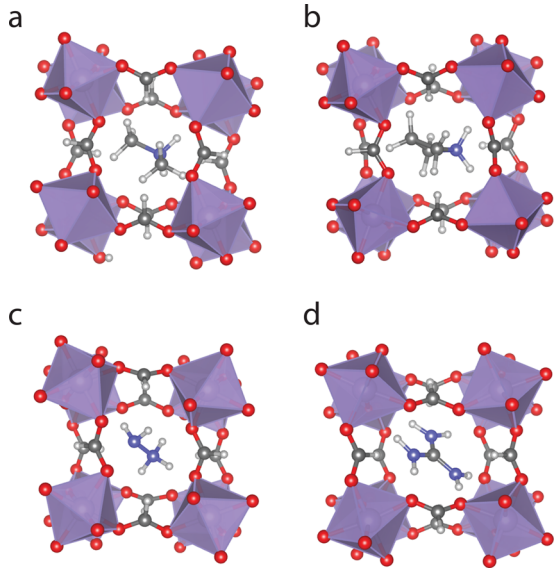

Figure 1. Perovskite-type unit cell of the formate-based perovskites studied in this work: (a) Dma$^+$, (b) Aze$^+$, (c) Hy$^+$, and (d) Gua$^+$. Zn is purple, O is red, N is blue, C is gray, and H is white.

The crystal structures of our four prototypical frameworks were optimized using density functional theory (DFT) with the PBEsol[22] exchange-correlation functional and the D3[23,24] correction to account for dispersion interactions. Full details of the computational setup and the optimized lattice parameters are given in the Supporting Information (SI).

To quantify the hydrogen bonding in the four different compounds we used the scheme shown in Figure 2. This method serves to remove the monopole term of the electrostatic interactions between the cation and the anionic framework so that the strength of the dipolar interaction and higher-order terms forming the hydrogen bond can be determined. Previous estimates of the hydrogen-bonding strength failed to account for the fact that the A site is charged.[18] Our method also explicitly removes any term involving the total energy of a charged supercell from the final energy, which means that it is not sensitive to the choice of supercell, as charged periodic DFT calculations can be (see SI section on supercell convergence).

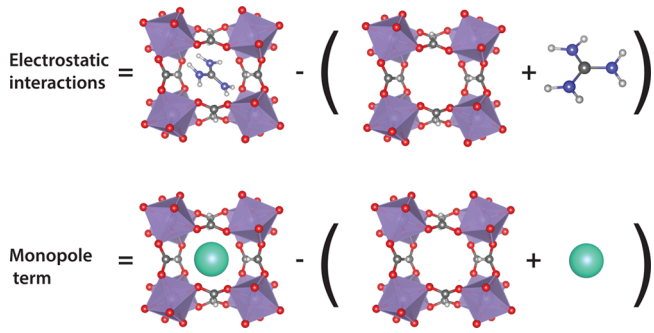

Figure 2. Schematic process for calculating the H-bonding interactions between the amine cation and the negatively charged $[Zn(HCOO)_3]^-$ cage. The upper panel shows the procedure for calculating the total electrostatic interactions, while the lower panel shows how to calculate the monopole term of this interaction. The difference between these two numbers arises from hydrogen bonding and higher order electrostatic interactions. Zn is purple, O is red, N is blue, C is gray, H is white, and Cs is cyan.

In our scheme, the total electrostatic energy of the interaction between A^+ and BX_3^- is calculated as the energy difference between the ABX_3 framework containing the A^+ cation and the separated cation and anionic BX_3^- framework, as illustrated in the upper panel of Figure 2. Note that the real unit cell contains several crystallographically dependent cations, but the symmetry is lowered to P1 and only one is removed. The monopole term of the interaction is calculated by replacing one of the molecular cations with Cs^+ at the center of the cage and repeating the above calculation, as shown in Figure 2 (lower panel). The structure is not relaxed following substitution. We define the hydrogen-bonding interaction as the difference between the total electrostatic interaction and the monopole interaction term, with results shown in Table 1 for the four compounds. We also give the total electrostatic energy (E_{tot}), the number of hydrogen-bond donor atoms (i.e., N−H bonds) per cation (n), each of which might be involved in one or more hydrogen bonds of varying strength, the temperature of the order−disorder phase transition (T_c), and the difference between calculated and measured ^{1}H NMR shifts ($\Delta\delta$, see below) for H-bonded hydrogen atoms.

The results reveal a higher total hydrogen-bonding energy in the **Gua**$^+$ and **Hy**$^+$ compounds than in the **Dma**$^+$ and **Aze**$^+$ compounds. The number of hydrogen-bonding centers correlates with the hydrogen -bonding energy in each material; that is, we find similar energies per center. For the four

DOI: 10.1021/acs.jpclett.7b03106
J. Phys. Chem. Lett. 2017, 8, 6154−6159

Table 1. Calculated Total Electrostatic Energy (E_{tot}) and Hydrogen-Bonding Energy ($E_{H\text{-}bond}$), Together with Related Properties[a]

	Gua^+	Hy^+	Aze^+	Dma^+
n	6	5	2	2
E_{tot} (eV)	7.61	7.96	6.97	7.06
$E_{H\text{-}bond}$ (eV)	1.29	1.40	0.42	0.36
$E_{H\text{-}bond}/n$ (eV)	0.21	0.28	0.21	0.18
T_c (K)	503[25] [b]	352[26]	299[27]	156[14]
$\Delta\delta$ (ppm)	1.7	1.5(NH_3) 1.6(NH_2)	2.1	2.3

[a]Number of hydrogen-bonding donors (n), cation ordering temperature (T_c), and the difference between calculated and measured ^{1}H NMR chemical shifts ($\Delta\delta$) of H-bonded hydrogen atoms. [b]Decomposition temperature; no phase transition observed.

materials considered here, each donor is involved in one short hydrogen bond (H−O distance <2.1 Å), which is expected to give the dominating contribution to the hydrogen-bonding energy, with smaller contributions from weaker hydrogen-bonding interactions of varying number and geometry. The similar hydrogen-bonding energies of ∼0.2 eV/bond are comparable to the values typically calculated for N−H−O hydrogen bonds, which gives us confidence in our approach. As an example, high-level quantum-chemical calculations give an energy of 0.38 eV (8.6 kcal/mol) for the two N−H−O hydrogen bonds formed between two peptide units, that is, 0.19 eV/bond.[28] The corresponding values calculated for formate perovskites in ref 18 did not remove the monopole term and give values of ∼0.8 eV/bond. We note that the monopole term varies in magnitude between the different compounds, as would be expected from the differences in cage size and shape (cf. Table 1).

To probe the validity of our model we performed solid-state ^{1}H NMR measurements, which gives information about cation dynamics. The combination of such experiments and DFT chemical shift calculations, that is, "NMR crystallography",[29−31] can be applied to refine the positions of hydrogen atoms in hybrid formate perovskites.[32] This approach relies on the sensitivity of ^{1}H chemical shifts to local structure, for example, bond lengths and hydrogen bonding. Furthermore, ^{1}H line widths in these compounds are dominated by ^{1}H−^{1}H dipolar couplings, with line widths reduced by motion of the A-site cation,[5] and the data thus gives information on cation dynamics. Solid-state magic-angle spinning (MAS) ^{1}H NMR spectra and peak assignments are shown in Figure 3a for the series of zinc formates. The formate resonances appear in the region of ∼8 to 9 ppm, and resonances from $R_2NH_2^+$/$R'NH_3^+$ groups appear at similar chemical ranges, with the large shifts indicative of hydrogen bonding with the zinc formate framework.

For the **Gua**$^+$ compound, the guanidinium N−H resonance is particularly broad, while the formate resonance is also broadened compared with the other compounds in the series. The broad line widths indicate a lack of motion in the **Gua**$^+$ compound, likely originating from hindered C−N bond rotation due to the delocalized guanidinium π bonding and the strong hydrogen bonds that keep the position of the cation fixed in the framework. Additionally, **Gua**$^+$ has a N lone pair that can potentially interact with the framework via hydrogen bonding; although these are weaker than N−H−O bonds, they can nonetheless also contribute to enhanced stability. This is

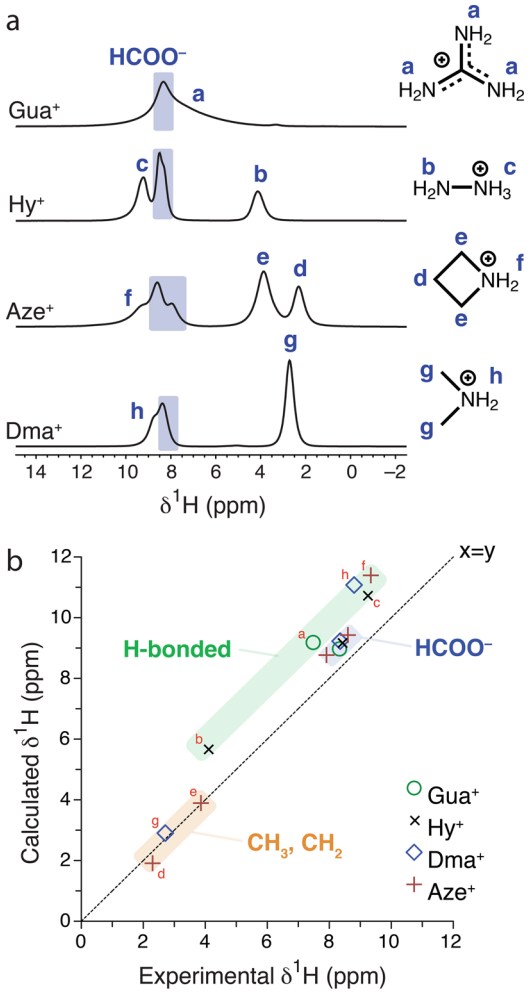

Figure 3. (a) ^{1}H MAS NMR (16.4 T, ^{1}H 700 MHz) spectra of [Am][Zn(HCOO)$_3$] hybrid perovskites. The sample spinning rate was 60 kHz in all cases except for the Aze^+ sample where a spinning rate of 36 kHz was used. Spectra were acquired without temperature control, and thus the sample temperatures are ∼317 ± 11 K, except for the measurements on the Aze^+, where we estimate a sample temperature of 298 ± 4 K. Note that these temperatures arise from frictional heating effects under MAS and were estimated from ^{207}Pb NMR measurements on lead nitrate at different spinning speeds.[34] (b) DFT-calculated chemical shifts plotted against the experimental values. The dashed line, $x = y$, indicates exact agreement between calculated and experimental values. Letters (in red) indicate the corresponding peak in the NMR spectrum as shown in panel a.

consistent with molecular dynamics simulations, which showed that the cation is not rotating at room temperature.[33]

We performed additional DFT calculations of the ^{1}H chemical shifts for the series of investigated compounds; cf. SI for details. The difference between calculated and measured chemical shifts can be related to the degree of mobility of molecular groups, and hence to hydrogen bonding strength. The results, Figure 3b, show good agreement between the calculated and measured shifts, especially for the CH_3, CH_2, and $HCOO^-$ groups, where the differences are <1 ppm. For the N−H hydrogen atoms, the calculated shifts are consistently larger than the experimental shifts. This is rationalized by noting that the calculations do not take into account the vibrational and rotational motion present at ambient temperature. This phenomenon is well known, and a number of

DOI: 10.1021/acs.jpclett.7b03106
J. Phys. Chem. Lett. 2017, 8, 6154−6159

Table 2. Calculated Total Electrostatic Energies (E_{tot}) and Hydrogen-Bonding Energies ($E_{H\text{-}bond}$) in a Series of Halide Perovskites, Together with Related Properties: Number of Hydrogen-Bonding Donors in the Cation (n) and Cation Ordering Temperature (T_c)

	$MaPbCl_3$	$MaPbBr_3$	$MaPbI_3$	$FaPbCl_3$	$FaPbBr_3$	$FaPbI_3$
n	3	3	3	4	4	4
E_{tot} (eV)	8.59	8.19	9.09	8.60	8.15	9.03
$E_{H\text{-}bond}$ (eV)	0.27	0.26	0.26	0.16	0.10	0.09
$E_{H\text{-}bond}/n$ (eV)	0.09	0.09	0.09	0.04	0.02	0.02
T_c (K)	173[44]	144[44]	162[44]	[a]	[a]	140[45]

[a]Transition temperatures were not found for the Cl and Br **Fa**$^+$ compounds.

approaches have been developed to account for the effects of motion.[35−41] The deviations between experimental and calculated shifts, $\Delta\delta = \delta_{DFT} - \delta_{Exp}$ (Table 1), indicate motion of the A-site cation, with the resulting reduction in effective hydrogen-bond strength, giving rise to lower experimental chemical shifts, and thus a larger $\Delta\delta$ indicates weaker hydrogen bonds. The values of $\Delta\delta$ are largest for hydrogens in the **Aze**$^+$ (2.1 ppm) and **Dma**$^+$ (2.3 ppm) compounds, while deviations are also observed for **Gua**$^+$ (1.7 ppm) and **Hy**$^+$ (1.5 and 1.6 ppm, for NH_3 and NH_2, respectively). These findings are consistent with the greater motion of the protonated amines in **Aze**$^+$ and **Dma**$^+$, disrupting hydrogen-bonding interactions due to thermally activated disorder. Indeed for **Dma**$^+$ NMR measurements were made above T_c, while for **Aze**$^+$ measurements were made close to T_c, and for **Gua**$^+$ and **Hy**$^+$ measurements were made below T_c. Future NMR measurements should be carried out to explore the temperature dependence of the NMR parameters above and below Tc.

Calculations of differences in NMR shifts between isolated molecules and molecules in molecular crystals have previously been used to probe hydrogen-bonding interactions.[42,43] We have performed similar calculations to verify the effects of hydrogen bonding on the NMR shifts of the molecules in the formate perovskites. Our results (shown in more detail in the SI) confirm the presence of strong hydrogen bonds between the NH groups and the frameworks with the exception of NH_2 in **Hy**$^+$.

Our results demonstrate a clear correlation between the calculated hydrogen-bonding strengths, the degree of motion indicated by the ^{1}H NMR measurements and the reported order−disorder phase-transition temperatures (given in Table 1). The **Gua**$^+$ compound, which is the only one for which an order−disorder transition is not reported below the decomposition temperature of 503 K,[25] has a high hydrogen-bonding energy, broad ^{1}H NMR lineshapes (even under fast MAS), and shows a small value of $\Delta\delta$. The **Hy**$^+$ compound likewise has a high hydrogen-bonding energy, and the cations are expected to be ordered at room temperature (phase transition at 352 K[26]). The ^{1}H NMR suggests that the hydrogen atoms are relatively fixed, although previous ^{1}H NMR investigations and molecular dynamics simulations have indicated that rotation of the NH_2 group around the N−N bond of the cation could be possible at the experimental temperatures.[32,33]

The **Aze**$^+$ and **Dma**$^+$ compounds have similar and significantly lower calculated hydrogen-bonding energies and a larger $\Delta\delta$, indicating a higher degree of motion. The **Aze**$^+$ cation undergoes ring-puckering above 299 K,[27,46] while the N-atom of the **Dma**$^+$ cation has been reported to jump between three equivalent positions by rotation of the molecule around the long axis of the molecule above 156 K.[14,47] The fact that the very similar hydrogen-bonding energies do not result in similar transition temperatures is probably related to the different nature of the transition. The barrier for rotation of the **Dma**$^+$ cation is associated with breaking of the hydrogen bonds,[48] while the barrier for the transition in the **Aze**$^+$ compound is also associated with the ring-puckering motion.

We now apply our scheme to six hybrid halide perovskites based on the methylammonium ($CH_3NH_3^+$, **Ma**$^+$) and formamidinium ($CH(NH_2)_2^+$, **Fa**$^+$) cations and the Cl, Br, and I halide atoms. These materials have been intensely studied due to their high efficiency as absorber-layers in thin-film solar cells.[49] They have low order−disorder transition temperatures of ∼150 K (cf. Table 2), and significant attention has been devoted to how the cation dynamics affects the photovoltaic performance through effects such as dipole alignment and electron−phonon coupling.[50]

The calculated hydrogen bonding energies for the halide perovskites are given in Table 2. Our results show no significant difference in the hydrogen bonding energy for the three different halides. The interaction is 0.10 to 0.15 eV stronger for the compounds based on **Ma**$^+$ than those based on **Fa**$^+$, even though **Fa**$^+$ has four N−H donor groups and **Ma**$^+$ only has three. An explanation for this is the larger permanent electric dipole on **Ma**$^+$ compared to **Fa**$^+$ (2.2D vs 0.2D as calculated for isolated molecules), which can lead to a larger induced dipole on the polarizable anions, as well as an additional dipole−dipole interaction between molecular cations in neighboring unit cells.[51]

The total hydrogen-bonding energies range from 0.09 to 0.27 eV in the halide perovskites, which is considerably lower than in the formate perovskites (0.36−1.40 eV). This is to be expected as N−H−O hydrogen bonds are generally considered to be stronger than N−H—X bonds. The weaker binding in the halide perovskites is furthermore consistent with the low order−disorder transition temperatures. The relative strengths of the hydrogen bonds in $FaPbX_3$ follow the series Cl > Br > I, which follows the order calculated for the interaction between an isolated cation and the halides (see the SI for further details). Interestingly there is no pronounced difference between the **Ma**$^+$ halides; this could be related to the stronger dipole in **Ma**$^+$, meaning that the differences in hydrogen-bond strengths are of the same order of magnitude as differences in dipole−dipole interactions caused by the removal of a molecule. Interestingly, the similarity in size of the halide and formate anions suggests that it might be possible to form a solid solution, as has previously been done with SCN^-,[52] and that this could be a route to tailor the order−disorder transition temperature in hybrid perovskites.

In conclusion, we have investigated the nature of the amine−cavity interactions in a number of hybrid perovskite materials. Our results show that hydrogen bonding is generally stronger in formate perovskites than in halide perovskites and that the A-

DOI: 10.1021/acs.jpclett.7b03106
J. Phys. Chem. Lett. 2017, 8, 6154−6159

site cations with stronger hydrogen bonding to the cavity have higher order−disorder transition temperatures. Our scheme for accessing the hydrogen-bonding strength is a clear improvement over previous schemes, and the approach can be easily extended to suit other framework materials. However, we note that a full picture must also include considerations about the order−disorder transition mechanism and associated steric interactions for the chosen shape of cation. Our study illustrates that ^{1}H NMR and DFT calculations are a powerful combination of techniques for quantifying the strength and effect of molecule−cavity interactions in the family of hybrid organic−inorganic perovskites. Complementary advances in experimental and theoretical approaches are expected to improve the description of cation dynamics, leading to further development of structure−property relationships.

■ ASSOCIATED CONTENT

Supporting Information

The Supporting Information is available free of charge on the ACS Publications website at DOI: 10.1021/acs.jpclett.7b03106.

Comparison of calculated and experimental unit cell parameters and further computational and experimental details. (PDF)

■ AUTHOR INFORMATION

Corresponding Author

*E-mail: K.T.Butler@bath.ac.uk.

ORCID

Katrine L. Svane: 0000-0003-1701-3476
Alexander C. Forse: 0000-0001-9592-9821
Clare P. Grey: 0000-0001-5572-192X
Anthony K. Cheetham: 0000-0003-1518-4845
Aron Walsh: 0000-0001-5460-7033
Keith T. Butler: 0000-0001-5432-5597

Present Address

▽A.C.F.: Department of Chemistry, Department of Chemical and Biomolecular Engineering, and Berkeley Energy and Climate Institute, University of California, Berkeley, CA.

Notes

The authors declare no competing financial interest.

DFT optimized structures and NMR data are available from https://doi.org/10.5281/zenodo.997350.

■ ACKNOWLEDGMENTS

K.L.S. is supported by ERC grant no. 277757. K.T.B. is funded by EPSRC (EP/M009580/1 and EP/J017361/1). We acknowledge computing support from the U.K. national supercomputing service (Archer) via membership of the U.K. Materials Chemistry Consortium, which is funded by EPSRC (EP/L000202), and from the University of Bath computing services (Balena). A.C.F. acknowledges the Sims Scholarship (Cambridge) for funding as well as John Griffin (Lancaster University) for support and useful discussions. A.C.F. and G.K. thank THMCRFC for support, and A.K.C. thanks the Ras al Khaimah Centre for Advanced Materials. Calculations in CASTEP were performed using the Darwin Supercomputer of the University of Cambridge High Performance Computing Service (http://www.hpc.cam.ac.uk/), provided by Dell, Inc. using Strategic Research Infrastructure Funding from the Higher Education Funding Council for England and funding from the Science and Technology Facilities Council.

■ REFERENCES

(1) Li, W.; Wang, Z.; Deschler, F.; Gao, S.; Friend, R. H.; Cheetham, A. K. Chemically Diverse and Multifunctional Hybrid Organic−Inorganic Perovskites. *Nat. Rev. Mater.* **2017**, *2*, 16099.

(2) Jain, P.; Ramachandran, V.; Clark, R. J.; Zhou, H. D.; Toby, B. H.; Dalal, N. S.; Kroto, H. W.; Cheetham, A. K. Multiferroic Behavior Associated with an Order-Disorder Hydrogen Bonding Transition in Metal-Organic Frameworks (MOFs) with the Perovskite ABX_3 Architecture. *J. Am. Chem. Soc.* **2009**, *131*, 13625−13627.

(3) Gómez-Aguirre, L. C.; Pato-Doldán, B.; Mira, J.; Castro-García, S.; Señaris-Rodriguez, M. A.; Sánchez-Andújar, M.; Singleton, J.; Zapf, V. S. Magnetic Ordering-Induced Multiferroic Behavior in $[CH_3NH_3]$-$[Co(HCOO)_3]$ Metal-Organic Framework. *J. Am. Chem. Soc.* **2016**, *138*, 1122−1125.

(4) Docampo, P.; Bein, T. A Long-Term View on Perovskite Optoelectronics. *Acc. Chem. Res.* **2016**, *49* (2), 339−346.

(5) Kieslich, G.; Kumagai, S.; Forse, A. C.; Sun, S.; Henke, S.; Yamashita, M.; Grey, C. P.; Cheetham, T. Tuneable Mechanical and Dynamical Properties in the Ferroelectric Perovskite Solid Solution $[NH_3NH_2]_{1-x}[NH_3OH]_x$ $Zn(HCOO)_3$. *Chem. Sci.* **2016**, *7*, 5108−5112.

(6) Chen, S.; Shang, R.; Wang, B.-W.; Wang, Z.-M.; Gao, S. An A-Site Mixed-Ammonium Solid Solution Perovskite Series of $[(NH_2NH_3)_x(CH_3NH_3)_{1-x}][Mn(HCOO)_3]$ (X = 1.00−0.67). *Angew. Chem.* **2015**, *127*, 11245−11248.

(7) Kieslich, G.; Goodwin, A. The Same and Not the Same: Molecular Perovskites and Their Solid-State Analogues. *Mater. Horiz.* **2017**, *4*, 362−366.

(8) Beecher, A. N.; Semonin, O. E.; Skelton, J. M.; Frost, J. M.; Terban, M. W.; Zhai, H.; Alatas, A.; Owen, J. S.; Walsh, A.; Billinge, S. J. L. Direct Observation of Dynamic Symmetry Breaking above Room Temperature in Methylammonium Lead Iodide Perovskite. *ACS Energy Lett.* **2016**, *1* (4), 880−887.

(9) Selig, O.; Sadhanala, A.; Müller, C.; Lovrincic, R.; Chen, Z.; Rezus, Y. L. A.; Frost, J. M.; Jansen, T. L. C.; Bakulin, A. A. Organic Cation Rotation and Immobilization in Pure and Mixed Methylammonium Lead-Halide Perovskites. *J. Am. Chem. Soc.* **2017**, *139* (11), 4068−4074.

(10) Collings, I. E.; Hill, J. A.; Cairns, A. B.; Cooper, R. I.; Thompson, A. L.; Parker, J. E.; Tang, C. C.; Goodwin, A. L. Compositional Dependence of Anomalous Thermal Expansion in Perovskite-like ABX_3 Formates. *Dalt. Trans.* **2016**, *45*, 4169−4178.

(11) Butler, K. T.; Walsh, A.; Cheetham, A. K.; Kieslich, G. Organised Chaos: Entropy in Hybrid Inorganic−Organic Systems and Other Materials. *Chem. Sci.* **2016**, *7* (10), 6316−6324.

(12) Butler, K. T.; Svane, K.; Kieslich, G.; Cheetham, A. K.; Walsh, A. Microscopic Origin of Entropy-Driven Polymorphism in Hybrid Organic-Inorganic Perovskite Materials. *Phys. Rev. B: Condens. Matter Mater. Phys.* **2016**, *94* (18), 180103.

(13) Wang, Z.; Hu, K.; Gao, S.; Kobayashi, H. Formate-Based Magnetic Metal-Organic Frameworks Templated by Protonated Amines. *Adv. Mater.* **2010**, *22* (13), 1526−1533.

(14) Jain, P.; Dalal, N.; Toby, B.; Kroto, H. W.; Cheetham, A. K. Order−Disorder Antiferroelectric Phase Transition in a Hybrid Inorganic−Organic Framework with the Perovskite Architecture. *J. Am. Chem. Soc.* **2008**, *130*, 10450−10451.

(15) Tian, Y.; Stroppa, A.; Chai, Y.; Yan, L.; Wang, S.; Barone, P.; Picozzi, S.; Sun, Y. Cross Coupling between Electric and Magnetic Orders in a Multiferroic Metal-Organic Framework. *Sci. Rep.* **2015**, *4* (1), 6062.

(16) Fu, D. W.; Zhang, W.; Cai, H. L.; Zhang, Y.; Ge, J. Z.; Xiong, R. G.; Huang, S. D.; Nakamura, T. A Multiferroic Perdeutero Metal-Organic Framework. *Angew. Chem., Int. Ed.* **2011**, *50* (50), 11947−11951.

(17) Di Sante, D.; Stroppa, A.; Jain, P.; Picozzi, S. Tuning the Ferroelectric Polarization in a Multiferroic Metal-Organic Network. *J. Am. Chem. Soc.* **2013**, *135*, 18126−18130.

(18) Li, W.; Thirumurugan, A.; Barton, P. T.; Lin, Z.; Henke, S.; Yeung, H. H. M.; Wharmby, M. T.; Bithell, E. G.; Howard, C. J.;

DOI: 10.1021/acs.jpclett.7b03106
J. Phys. Chem. Lett. 2017, 8, 6154−6159

Cheetham, A. K. Mechanical Tunability via Hydrogen Bonding in Metal-Organic Frameworks with the Perovskite Architecture. *J. Am. Chem. Soc.* **2014**, *136* (22), 7801−7804.
(19) Jeffrey, G. A.; Saenger, W. *Hydrogen Bonding in Biological Structures*; Springer: Berlin, 1991.
(20) Coulson, C. A. *Valence*; Oxford University Press: London, 1952.
(21) Steiner, T. The Hydrogen Bond in the Solid State. *Angew. Chem., Int. Ed.* **2002**, *41* (1), 48−76.
(22) Perdew, J. P.; Ruzsinszky, A.; Csonka, G. I.; Vydrov, O. A.; Scuseria, G. E.; Constantin, L. A.; Zhou, X.; Burke, K. Restoring the Density-Gradient Expansion for Exchange in Solids and Surfaces. *Phys. Rev. Lett.* **2008**, *100* (13), 136406.
(23) Grimme, S.; Antony, J.; Ehrlich, S.; Krieg, H. A Consistent and Accurate Ab Initio Parametrization of Density Functional Dispersion Correction (DFT-D) for the 94 Elements H-Pu. *J. Chem. Phys.* **2010**, *132* (15), 154104.
(24) Grimme, S.; Ehrlich, S.; Goerigk, L. Effect of the Damping Function in Dispersion Corrected Density Functional Theory. *J. Comput. Chem.* **2011**, *32* (16), 1456−1465.
(25) Hu, K.-L.; Kurmoo, M.; Wang, Z.; Gao, S. Metal-Organic Perovskites: Synthesis, Structures, and Magnetic Properties of $[C(NH_2)_3][M(II)(HCOO)_3]$ (M = Mn, Fe, Co, Ni, Cu, and Zn; $C(NH_2)_3$ = Guanidinium). *Chem. - Eur. J.* **2009**, *15* (44), 12050−12064.
(26) Chen, S.; Shang, R.; Hu, K.-L.; Wang, Z.-M.; Gao, S. $[NH_2NH_3][M(HCOO)_3]$ (M = Mn^{2+}, Zn^{2+}, Co^{2+} and Mg^{2+}): Structural Phase Transitions, Prominent Dielectric Anomalies and Negative Thermal Expansion, and Magnetic Ordering. *Inorg. Chem. Front.* **2014**, *1*, 83−98.
(27) Asaji, T.; Ito, Y.; Seliger, J.; Zagar, V.; Gradisek, A.; Apih, T. Phase Transition and Ring-Puckering Motion in a Metal-Organic Perovskite $[(CH_2)_3NH_2][Zn(HCOO)_3]$. *J. Phys. Chem. A* **2012**, *116*, 12422−12428.
(28) Řezáč, J.; Riley, K. E.; Hobza, P. S66: A Well-Balanced Database of Benchmark Interaction Energies Relevant to Biomolecular Structures. *J. Chem. Theory Comput.* **2011**, *7* (8), 2427−2438.
(29) Harris, R. Crystallography and NMR: An Overview. *Encyclopedia of Magnetic Resonance* **2008**, 1−13.
(30) Bonhomme, C.; Gervais, C.; Babonneau, F.; Coelho, C.; Pourpoint, F.; Azais, T.; Ashbrook, S. E.; Griffin, J. M.; Yates, J. R.; Mauri, F.; et al. First-Principles Calculation of NMR Parameters Using the Gauge Including Projector Augmented Wave Method: A Chemists Point of View. *Chem. Rev.* **2012**, *112* (11), 5733−5779.
(31) Martineau, C. NMR Crystallography: Applications to Inorganic Materials. *Solid State Nucl. Magn. Reson.* **2014**, *63*, 1−12.
(32) Kieslich, G.; Forse, A. C.; Sun, S.; Butler, K. T.; Kumagai, S.; Wu, Y.; Warren, M. R.; Walsh, A.; Grey, C. P.; Cheetham, A. K. The Role of Amine-Cavity Interactions in Determining the Structure and Mechanical Properties of the Ferroelectric Hybrid Perovskite $[NH_3NH_2]Zn(HCOO)_3$. *Chem. Mater.* **2016**, *28*, 312−317.
(33) Svane, K. L.; Walsh, A. Quantifying Thermal Disorder in Metal−Organic Frameworks: Lattice Dynamics and Molecular Dynamics Simulations of Hybrid Formate Perovskites. *J. Phys. Chem. C* **2017**, *121* (1), 421−429.
(34) Beckmann, P. A.; Dybowski, C. A Thermometer for Nonspinning Solid-State NMR Spectroscopy. *J. Magn. Reson.* **2000**, *146* (2), 379−380.
(35) Bryce, D. L. NMR Crystallography: Structure and Properties of Materials from Solid-State Nuclear Magnetic Resonance Observables. *IUCrJ* **2017**, *4*, 350−359.
(36) Ashbrook, S. E.; McKay, D. Combining Solid-State NMR Spectroscopy with First-Principles Calculations − a Guide to NMR Crystallography. *Chem. Commun.* **2016**, *52* (45), 7186−7204.
(37) Dračínský, M.; Bouř, P.; Hodgkinson, P. Temperature Dependence of NMR Parameters Calculated from Path Integral Molecular Dynamics Simulations. *J. Chem. Theory Comput.* **2016**, *12* (3), 968−973.
(38) Dračínský, M.; Hodgkinson, P. Effects of Quantum Nuclear Delocalisation on NMR Parameters from Path Integral Molecular Dynamics. *Chem. - Eur. J.* **2014**, *20* (8), 2201−2207.
(39) Hofstetter, A.; Emsley, L. Positional Variance in NMR Crystallography. *J. Am. Chem. Soc.* **2017**, *139* (7), 2573−2576.
(40) Li, X.; Neumann, M. A.; Van De Streek, J. The Application of Tailor-Made Force Fields and Molecular Dynamics for NMR Crystallography: A Case Study of Free Base Cocaine. *IUCrJ* **2017**, *4*, 175−184.
(41) Monserrat, B.; Needs, R. J.; Pickard, C. J. Temperature Effects in First-Principles Solid State Calculations of the Chemical Shielding Tensor Made Simple. *J. Chem. Phys.* **2014**, *141* (13), 134113.
(42) Yates, J. R.; Pham, T. N.; Pickard, C. J.; Mauri, F.; Amado, A. M.; Gil, A. M.; Brown, S. P. An Investigation of Weak CH···O Hydrogen Bonds in Maltose Anomers by a Combination of Calculation and Experimental Solid-State NMR Spectroscopy. *J. Am. Chem. Soc.* **2005**, *127* (29), 10216−10220.
(43) Uldry, A. C.; Griffin, J. M.; Yates, J. R.; Pérez-Torralba, M.; Santa María, M. D.; Webber, A. L.; Beaumont, M. L. L.; Samoson, A.; Claramunt, R. M.; Pickard, C. J.; et al. Quantifying Weak Hydrogen Bonding in Uracil and 4-Cyano-4′- Ethynylbiphenyl: A Combined Computational and Experimental Investigation of NMR Chemical Shifts in the Solid State. *J. Am. Chem. Soc.* **2008**, *130* (3), 945−954.
(44) Poglitsch, A.; Weber, D. Dynamic Disorder in Methylammoniumtrihalogenoplumbates (II) Observed by Millimeter-Wave Spectroscopy. *J. Chem. Phys.* **1987**, *87* (11), 6373−6378.
(45) Fabini, D. H.; Stoumpos, C. C.; Laurita, G.; Kaltzoglou, A.; Kontos, A. G.; Falaras, P.; Kanatzidis, M. G.; Seshadri, R. Reentrant Structural and Optical Properties and Large Positive Thermal Expansion in Perovskite Formamidinium Lead Iodide. *Angew. Chem., Int. Ed.* **2016**, *55* (49), 15392−15396.
(46) Imai, Y.; Zhou, B.; Ito, Y.; Fijimori, H.; Kobayashi, A.; Wang, Z.-M.; Kobayashi, H. Freezing of Ring-Puckering Molecular Motion and Giant Dielectric Anomalies in Metal-Organic Perovskites. *Chem. - Asian J.* **2012**, *7* (12), 2786−2790.
(47) Besara, T.; Jain, P.; Dalal, N. S.; Kuhns, P. L.; Reyes, A. P.; Kroto, H. W.; Cheetham, A. K. Mechanism of the Order-Disorder Phase Transition, and Glassy Behavior in the Metal-Organic Framework $[(CH_3)_2NH_2]Zn(HCOO)_3$. *Proc. Natl. Acad. Sci. U. S. A.* **2011**, *108* (17), 6828−6832.
(48) Duncan, H. D.; Dove, M. T.; Keen, D. A.; Phillips, A. E. Local Structure of the Metal-Organic Perovskite Dimethylammonium Manganese(II) Formate. *Dalt. Trans.* **2016**, *45*, 4380−4391.
(49) Stranks, S. D.; Snaith, H. J. Metal-Halide Perovskites for Photovoltaic and Light-Emitting Devices. *Nat. Nanotechnol.* **2015**, *10* (5), 391−402.
(50) Frost, J. M.; Walsh, A. What Is Moving in Hybrid Halide Perovskite Solar Cells? *Acc. Chem. Res.* **2016**, *49* (3), 528−535.
(51) Frost, J. M.; Butler, K. T.; Walsh, A. Molecular Ferroelectric Contributions to Anomalous Hysteresis in Hybrid Perovskite Solar Cells. *APL Mater.* **2014**, *2* (8), 081506.
(52) Chen, Y.; Li, B.; Huang, W.; Gao, D.; Liang, Z. Efficient and Reproducible $CH_3NH_3PbI_{3-x}(SCN)_x$ Perovskite Based Planar Solar Cells. *Chem. Commun.* **2015**, *51* (60), 11997−11999.

DOI: 10.1021/acs.jpclett.7b03106
J. Phys. Chem. Lett. 2017, 8, 6154−6159